Id.: EN47

NEUTRONICS EVALUATION FOR COATING LAYERS OF THE BLANKET SYSTEM IN A HYBRID FUSION-FISSION REACTOR

Natália G. P. L. Oliveira, Carlos E. Velasquez and Claubia Pereira

Departamento de Engenharia Nuclear
Universidade Federal de Minas Gerais - UFMG
Av. Antonio Carlos, 6627 Pampulha
31270-901, Belo Horizonte, MG, Brazil
nataliagplofis@gmail.com

Palavras-Chave: Fusion-Fission Hybrid, ITER, Coating Layers, Albedo, Transmutation

ABSTRACT

A hybrid fusion-fission reactor (FFH) can be understood as a large source of fusion neutrons combined with a layer of fissile fuel, which can be used both for the breeding of fissile material and for the transmutation of high-level radioactive waste (HLW), such as the long half-life actinide elements. To evaluate an FFH reactor for the transmutation of reprocessed fuel, two models of an FFH are analyzed: a simpler model for the plasma chamber without the representation of the divertor component (Model 1) and a model with the divertor component represented in a simplified form (Model 2). This work aims to analyze changes in the spectrum of fusion neutrons that reach the transmutation layers (TL) position in the two simulated FFH reactor models, investigating the albedo coefficients calculated through the input and output currents in the beryllium coating layers, heat absorber, and tritium production. Differences in the interactions of neutrons with these three layers are observed between the models, initially caused by the scattering of fusion neutrons with the W nuclei of the diverter's PFC, which can ultimately impact the transmutation rate between models.

1. INTRODUCTION

A hybrid fusion-fission reactor (FFH) can be understood as a fusion reactor combined with a layer of nuclear fuel from fission plants such as LWRs. This hybrid reactor might produce fissile material by capturing neutrons in fertile material, such as ^{238}U and ^{232}Th, present in fissile fuel, viable due to the availability of neutrons from the fusion source.

In addition, the high energy neutron flux provided by the fusion neutron source could be used to transmute minor actinides, which pose high radioactivity and long-term half-life. Therefore, providing a strategy to reduce the long half-life and transmute the minor actinides into fission products through fission, otherwise, they would be stored for millennia in high-level radioactive waste repositories (HLWRs) [1].

The Department of Nuclear Engineering at Universidade Federal de Minas Gerais (DEN/UFMG) has been studying and simulating different nuclear reactors and hybrid systems to study alternatives to reduce, recycle, and reuse the nuclides in the uranium and thorium nuclear fuels cycle. Therefore, the DEN/UFMG has been proposed a FFH based on the dimensions and materials proposed by ITER [2], introducing a transmutation layer (TL) into the system [3]. Furthermore, this work introduces modifications to approach the model to a real tokamak system by adding a divertor component to the plasma chamber of the fusion system, also based on the ITER projector [4]. The divertor component, located at the bottom of the vacuum chamber, extracts the heat and ash produced by fusion reactions, thus minimizing plasma contamination and protecting the layers of surrounding materials from high thermal and

neutronic loads. Based on international research and development efforts, Tungsten was chosen as a shielding material to sustain these high heat loads [5-7].

This work aims to analyze changes in the spectrum of fusion neutrons that reach the transmutation layer of the simulated FFH reactor after the insertion of the divertor component. To this end, two models for the FFH reactor were compared, with and without this component, and the neutron spectrum in the layers internal to the TL and their interactions with the constituent materials were examined. Such analyses were conducted with the MCNP6.2 code in steady state.

2. METHODOLOGY

2.1. FFH reactor: Fusion device parameters and components

The model for the FFH reactor developed at DEN/UFMG is based on the materials and radial dimensions proposed by ITER [2] but with some modifications in dimensions to introduce a transmutation layer into the system [3]. Fig. 1 shows the three-dimensional modeling of the FFH reactor without the Divertor component (Model 1), where its geometry is represented by the intersection of cylinders and planes limiting the different layers of materials.

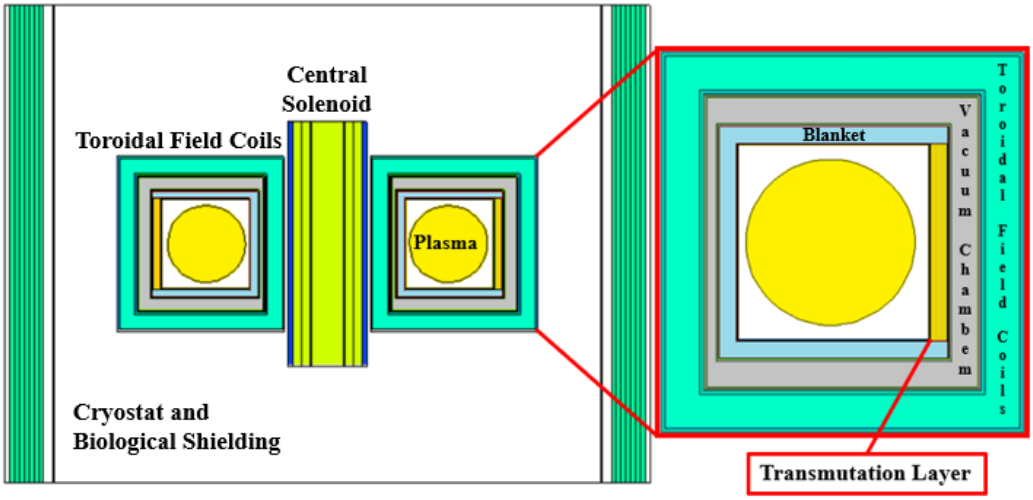

Fig. 1. Axial and radial sections Model 1 of the FFH reactor.

The main plasma parameters used for the fusion device were based on [8], as presented in Tab. 1. The ^{2}H-^{3}H plasma is maintained at a temperature of 10 keV for fusion reactions to occur, where after the interaction, an alpha particle and a neutron are produced with energies of approximately 3.5 MeV and 14.1 MeV, respectively. For the FFH reactor models (with and without the Divertor component), the energy spectrum of the fusion neutrons is governed by the Gaussian energy spectrum

$$p(E) = C \exp[-((E - b)/a^2)] \,, \tag{1}$$

described with the SDEF source definition card of the MCNP6.2 code, with a being the width ΔE above b where the exponential value is equivalent to e^{-1} and b, the parameter that defines the average energy. The values of a and b provided by the code for ^{2}H-^{3}H fusion at a temperature of 10 keV are -0.01 MeV and -1.00 MeV, respectively. The values for the fusion power and volume of the Plasma Chamber, 500 MW, and 837.00 m3, respectively, are based on the ITER Tokamak [2].

Tab. 1. Plasma parameters for ITER-based FFH reactor fusion device.

Parameters	
Minor Radius (m)	2.00
Major Radius (m)	6.21
Plasma Elongation	1.85
Plasma Temperature (keV)	10.00
Plasma Type	^{2}H-^{3}H
Plasma Chamber Volume	837.00
Fusion Power (MW)	250-500
Fission Power (MW)	3000

2.2. Divertor Component

In this work, a geometrically more simplified modeling of the Divertor component was carried out for the FFH reactor (Model 2) to obtain results with fewer errors in the simulations caused by losses in particle tracking by the code due to the complexity of the geometry. Fig. 2 shows the FFH reactor's two-dimensional modeling with this Divertor component model. It is composed of intersections of flat and cylindrical surfaces. As a simplified representation, only its main structural and coating layers were modeled, as shown in Tab. 2. 102 surfaces were used for its model with the code MCNP6.2. Even with the insertion of the diverter component, the volume of the plasma chamber and the dimensions of the major and minor radii remained unchanged.

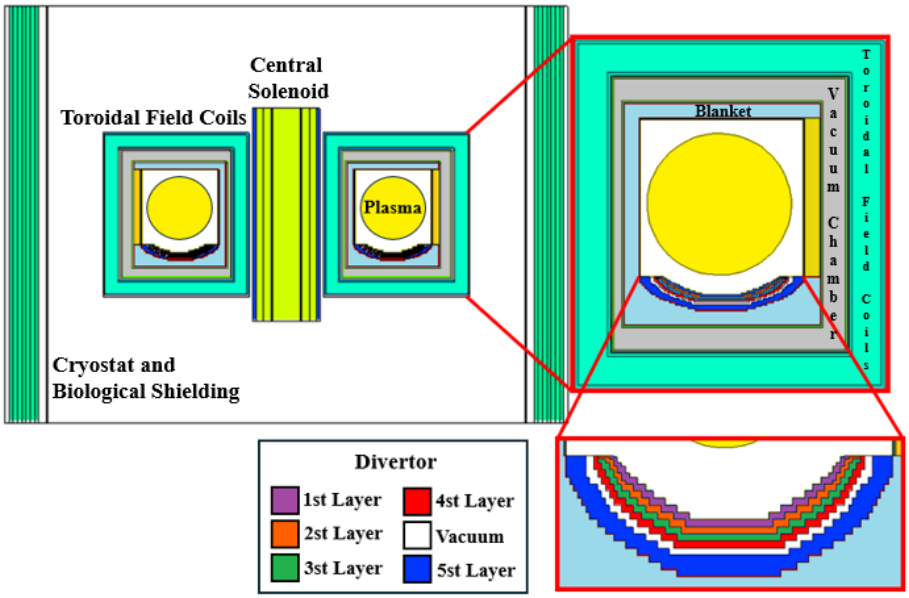

Fig. 2. Axial and radial sections Model 2 of the FFH reactor.

Tab. 2. Diverter component modeling specifications for Model 2 of the FFH reactor.

Components	**Composition**
1st Layer	W-1.1%TiC
2nd Layer	Cu
3rd Layer	CuCrZr
4st Layer	55% SS316L(N)-IG + 45% water
5st Layer	65% SS316L(N)-IG + 35% water

2.3. Calculation for the Neutron Current

To verify the influence of the Divertor component on the transport and energy of fusion neutrons that reach the transmutation layer in the new modeling of the FFH reactor, calculations of the albedo coefficient were carried out on the surfaces that make up the blanket system before TL, for both models without and with the Divertor component (Models 1 and 2, respectively). From the definition of the albedo coefficient

$$\alpha \equiv \frac{J_-}{J_+} , \tag{2}$$

the positive (input current in the respective coating layer) and negative (output current in the respective coating layer) currents of fusion neutrons crossing the cylindrical surfaces of the analyzed coating layers (Fig. 3) are calculated

$$J_\pm = \int dE \int dt \int dA \int_{\substack{\hat{\Omega}\cdot\hat{n}<0 \\ \hat{\Omega}\cdot\hat{n}>0}} d\,\hat{\Omega}\,|\hat{\Omega}\cdot\hat{n}|\psi(\vec{r},\hat{\Omega},E,t) \tag{3}$$

where J_+ corresponds to the angular interval $-1 \leq \mu < 0$ and J_-, $0 < \mu \leq 1$ being $\mu = \hat{\Omega}\cdot\hat{n}$, cosine of the angle between the normal to the surface $\hat{n}$ and the trajectory of the particle $\hat{\Omega}$.

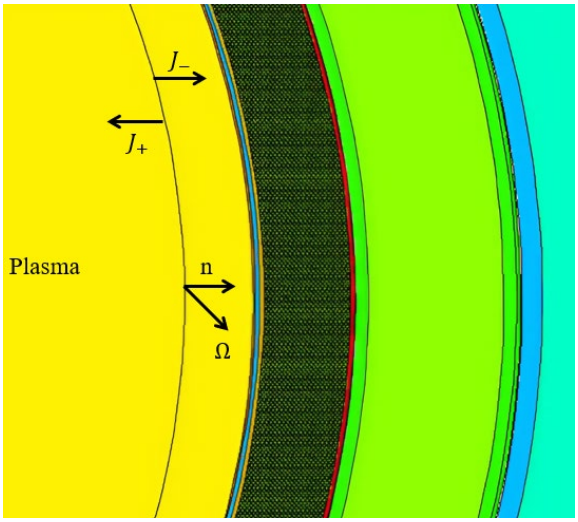

Fig. 3. Representation for calculating neutron current.

3. RESULTS

Fig. 4 presents the location of the blanket system's coating layers for models 1 and 2. The first coating layer, composed of the Be-S65C alloy, has a thickness of 1.0 cm and a volume of 2.39 m^3, as shown in Tab. 3, also specifying its composition and density used in the simulations. This alloy has neutron multiplier properties (probability of occurrence of (n,2n) reactions, especially with the ^{9}Be isotopes, for high-energy neutrons). It is also a moderator, altering the fusion neutron spectrum from the plasma chamber.

The second coating layer, composed of the CuCrZr-IG alloy and whose composition is presented in Tab. 3, has the function of absorbing the heat generated by collisions of plasma particles with the first coating layer (Be-S65C) of the blanket system, thus avoiding greater wear on the structure. The copper in its composition acts as an efficient heat sink, and the addition of chromium and zirconium increases resistance to deformation, mechanical wear, and

corrosion [2], properties necessary to withstand the high temperatures and pressures in the tokamak.

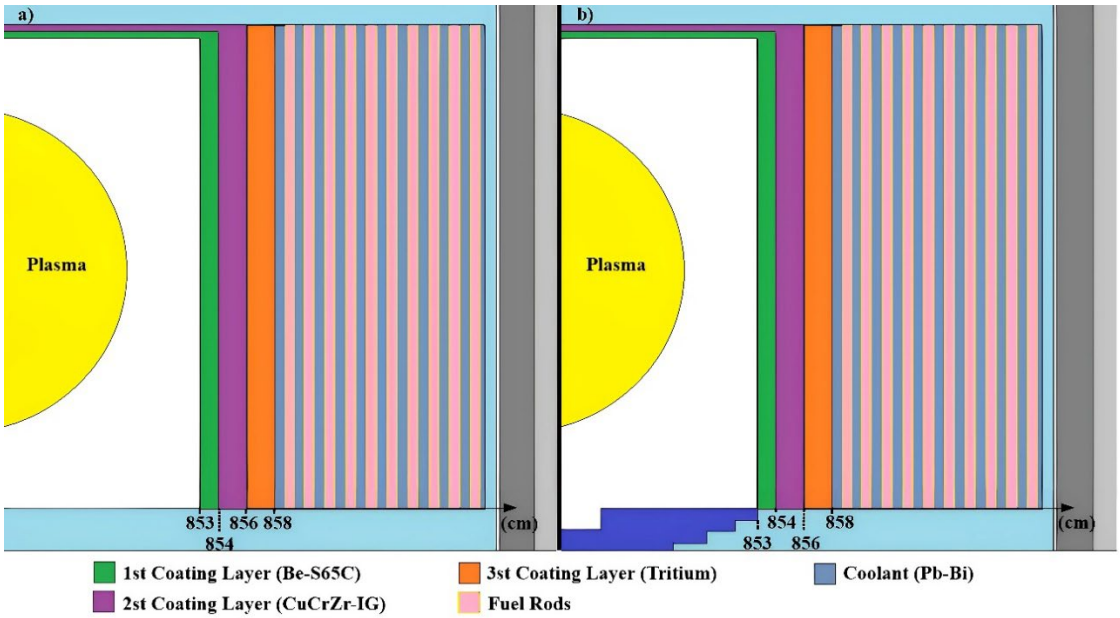

Fig. 4. Location of the Blanket System coating layers for a) Model 1 and b) Model 2.

Tab. 3. Composition for the coating layers of the blanket system in the models.

	1st Coating Layer		**2nd Coating Layer**		**3th Coating Layer**	
Atomic Fraction	^{9}Be	9.95508E-01	^{16}O	7.93427E-05	^{6}Li	2.25766E-01
	^{12}C	5.42644E-06	^{52}Cr	1.09950E-02	^{6}Li	7.74234E-01
	^{16}O	4.46127E-03	^{63}Cu	6.89778E-01	-	-
	^{24}Mg	3.01657E-07	^{65}Cu	2.97981E-01	-	-
	^{27}Al	1.34078E-06	^{90}Zr	1.05869E-03	-	-
	^{28}Si	1.16377E-06	^{96}Zr	2.77877E-05	-	-
	^{56}Fe	1.03481E-06	^{114}Cd	8.00253E-05	-	-
	^{58}Ni	2.10296E-05	-	-	-	-
	^{238}U	4.55905E-08	-	-	-	-
Atomic Density (atoms/b.cm)	1.23044E-01		8.47760E-02		4.31030E-02	
Position (m)	8.53 to 8.54		8.54 to 8.56		8.56 to 8.58	
Volume (m^3)	2.39		4.79		4.81	

The tritium used in fusion reactions is obtained mainly from the capture of neutrons by the isotopes of ^{6}Li and ^{7}Li, the latter with a lower probability of occurrence. For ^{6}Li, the highest probabilities occur for low-energy neutrons for the intermediate energy range. In previous works [9], studies were carried out to insert such a layer to take advantage of the low-energy neutrons scattered by the innermost surrounding layers. Tab. 3 presents more details about the layers, such as composition, atomic density, and volume.

The analysis of the albedo for a cylindrical surface with a radius of 853.0 cm (Fig. 5) reveals that the neutrons leaving the plasma chamber and reaching this surface are predominantly 14.1 MeV neutrons in both models. A distinction between the models occurs in the intermediate energy range (1.0 eV < E < 1.0 MeV) and thermal energy range (E < 1.0 eV). The total albedo

coefficient calculated for the surface (Tab. 4) shows that Model 1 exhibits a higher escape of fusion neutrons than Model 2, with a difference of approximately 5%. This higher albedo coefficient in Model 1 is associated with the escape of fast neutrons, which results in a more hardened energy spectrum within the volume of the layer, as indicated by the calculated average energy values ($\bar{E}$) in Tab. 4. In contrast, in Model 2, a larger percentage of neutrons in the intermediate energy range (1.0 eV < E < 1.0 MeV) — approximately 33% compared to 25% in Model 1 — corresponds to the observed peak in the albedo coefficient for the cylindrical surface with a radius of 853.0 cm (Fig. 5).

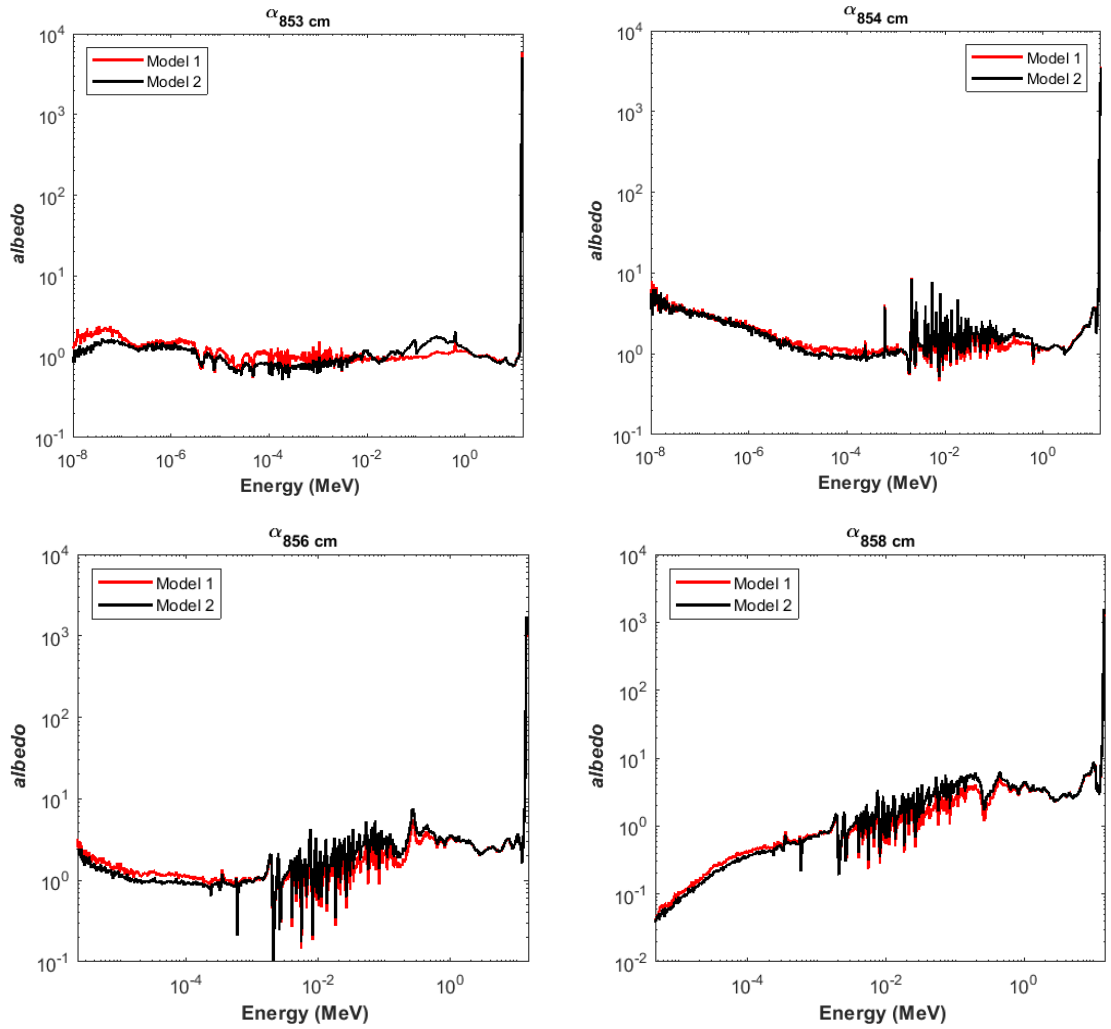

Fig. 5. Albedo for cylindrical surfaces with radii 853.0 cm, 854.0 cm, 856.0 cm, and 858.0 cm, delimiting the coating layers of Models 1 and 2.

For the albedo on the cylindrical surface with a radius of 854.0 cm, most neutrons escaping to the second coating layer remain high-energy neutrons. However, the graph now shows an increase in the leakage current ($J_{-}^{854\ cm}$) of thermal-energy neutral particles due to scattering interactions with isotopes of ^{9}Be, the primary constituent of the first coating layer (Tab. 3). The light mass of the ^{9}Be nucleus allows it to remove up to 18% of the neutron's initial energy in elastic collisions, expressed as $\overline{\Delta E}/E = {}^{1}/_{2}\,(1-\alpha)$, where α is called the collision parameter, given by $\alpha = (\bar{A}-1/\bar{A}+1)^2$ [10]. Consequently, the increased number of capture reactions in the layer correlates with the significant decrease in particle flux within this energy range, as seen in Tab. 4. This reduction in flux also results in a decrease in the average energy of neutral

particles within the layer, more pronounced in Model 1 (about 7%) and with a smaller decrease in Model 2 (around 1%).

Tab. 4. Calculated values for currents and flux in the coating layers of the models.

			Model 1	**Model 2**
albedo		853 cm	2.00	1.90
		854 cm	2.24	2.16
		856 cm	3.27	3.30
		858 cm	2.24	2.17
1st Coating Layer	$\phi\ (n/cm^2.s)$	Thermal	1.63E+12	1.63E+12
		Intermediate	2.85E+13	5.24E+13
		Fast	8.34E+13	1.05E+14
		Total	1.13E+14 $\pm$0.05%	1.59E+14 $\pm$0.05%
		$\bar{E}$ (MeV)	4.32	3.20
2nd Coating Layer	$\phi\ (n/cm^2.s)$	Thermal	6.56E+11	6.71E+11
		Intermediate	2.41E+13	4.07E+13
		Fast	7.46E+13	8.75E+13
		Total	9.93E+13 $\pm$ 0.05%	1.29E+14 $\pm$ 0.04%
		$\bar{E}$ (MeV)	4.01	3.16
3th Coating Layer	$\phi\ (n/cm^2.s)$	Thermal	3.76E+11	5.03E+11
		Intermediate	2.08E+13	3.28E+13
		Fast	5.76E+13	6.46E+13
		Total	7.88E+13 $\pm$ 0.06%	9.79E+13 $\pm$ 0.05%
		$\bar{E}$ (MeV)	4.00	3.28

For the albedo coefficients of the cylindrical surface at a radius of 856.0 cm, an increase in the escape of both thermal and fast neutrons to the subsequent coating layer is observed relative to the previous surface ($\alpha_{854\ cm}$). Although the second coating layer is composed of heavier elements than the beryllium alloy—such as copper, chromium, and zirconium—where approximately 3% of the neutron's energy is lost in collisions with these nuclei ($\overline{\Delta E}/E$), scattering reactions remain the dominant interactions in this layer, thereby reducing particle energy while diffusing them throughout the system. As a result, it can be concluded that capture reactions in this layer are less frequent, and given the heavier mass of these nuclides, inelastic scattering reactions, such as (n,2n), are more likely to occur, leading to the release of high-energy neutrons. The particle flux decreases in both models by approximately 13% to 19%, relative to the first cladding layer, although the average energy loss is greater in Model 1 (about 7%).

Finally, for the cylindrical surface with a radius of 858.0 cm, there is a decline in the thermal neutron leakage current, as well as a reduction in the peak corresponding to the point of maximum energy. These changes indicate the occurrence of low-energy neutron capture reactions by ^{6}Li nuclei, subsequently decaying into ^{3}H and an alpha particle, as well as the moderation of high-energy neutrons, since the maximum percentage value of energy that the neutron loses in an elastic collision with ^{6}Li and ^{7}Li nuclei can reach 22% of its initial energy [10]. It is observed that Model 2 exhibits a higher flux of thermal neutrons, leading to a greater likelihood of ^{3}H production. However, the average neutron energy within the volume of this layer is lower in Model 2 compared to Model 1, which implies a reduced transmutation rate by the fission of reprocessed fuel in the transmutation layer. This is supported by the softer energy spectrum of the leakage current, $\underline{J}^{858\ cm}$, in Model 2.

4. CONCLUSION

With the insertion of the divertor component in Model 2, it starts to act as a reflector of fusion neutrons, increasing the intensity of the current of particles that cross the walls of the systems, however, at lower energies. The increase in particle intensity impacts the rates of elastic scattering reactions in the analyzed layers, which, as a consequence, can contribute to tritium production in the third coating layer. In contrast, in Model 1, with a slightly more hardened neutron spectrum, reactions with the production of secondary particles and inelastic scattering can occur more frequently in the layers analyzed, indicating an increase in the activation of the materials. However, the hardness spectrum makes it possible to consume transuranic through fission in TL. Model 2 is adopted for future analyses of the ITER-based hybrid reactor, where the aim is to improve the model geometry, properly evaluating the burnup of reprocessed fuel in the TL.

ACKNOWLEDGMENTS

The authors are grateful to the Brazilian research funding agencies, Comissão Brasileira de Energia Nuclear - CNEN (Brazil), Conselho Brasileiro de Desenvolvimento Científico e Tecnológico - CNPq (Brazil), Coordenação de Aperfeiçoamento de Pessoal de Nível Superior - CAPES (Brazil) and Fundação de Amparo à Pesquisa do Estado de Minas Gerais - FAPEMIG (MG/Brazil) for the support.

REFERENCES

[1] H. Nifenecker *et al.*, Accelerator Driven Subcritical Reactors, Bristol and Philadelphia, Institute of Physics Publishing (2003).

[2] IAEA, Summary of the ITER final design report July 2001, International Atomic Energy Agency (IAEA) (2001), http://inis.iaea.org/search/search.aspx?orig_q=RN:33001691.

[3] C. E. Velasquez *et al*., Fusion–Fission Hybrid Systems for Transmutation, *Journal of Fusion Energy*, Vol 35 – Number 1, pp. 1-134 (2016).

[4] Natália G. P. L. Oliveira *et al.*, Fusion-Fission Hybrid System – Layer Transmutation Analysis After Divertor Insertion, Anais da Semana Nacional de Engenharia Nuclear e da Energia e Ciências das Radiações, Belo Horizonte, 24-26 may online event (2021). Available in: https//www.even3.com.br/anais/advs2021/459173-FUSION-FISSION-HYBRID-SYSTEM--LAYER-TRANSMUTATION-ANALYSIS-AFTER-DIVERTOR-INSERTION. Accessed in: 06/09/2024.

[5] E. Tsitrone, *et al*., Investigation of plasma wall interactions between tungsten plasma facing components and helium plasmas in the WEST tokamak, *Nucl. Fusion*, Vol. 62, pp. 076028 (2022), https://dx.doi.org/10.1088/1741-4326/ac2ef3

[6] Ch. Linsmeier *et al.*, Development of advanced high heat flux and plasma-facing materials, *Nucl. Fusion*, Vol. 57, pp. 60 (2017), https://doi.org/10.1088/1741-4326/aa6f71

[7] M. Missirlian *et al*., Manufacturing, testing and installation of the full tungsten actively cooled ITER-like divertor in the WEST tokamak, *Fusion Engineering and Design*, Vol. 193, pp. 113683 (2023), https://doi.org/10.1016/j.fusengdes.2023.113683

[8] W. M. Stacey *et al.*, A fusion transmutation of waste reactor, *Fusion Engineering and Design*, Vol. 63–64, n. 64, pp. 81–86 (2002).

[9] R.V.A. Marques *et al.*, Tritium Breeder Layer Evaluation of Fusion-Fission Hybrid System, *Fusion Science and Technology*, Vol. 76, pp. 145-152 (2020).

[10] John R. Lamarsh and Anthony J. Baratta, Introduction to Nuclear Engineering, 3th ed., New Jersey, Prentice-Hall (2001).